Pergamon

0301-9322(95)00022-4

Int. J. Multiphase Flow Vol. 21, No. 5, pp. 875–892, 1995

0301-9322/95 $9.50 + 0.00

ISOTHERMAL DRYING OF NON-HYGROSCOPIC CAPILLARY-POROUS MATERIALS AS AN INVASION PERCOLATION PROCESS

M. PRAT

Institut de Mécanique des Fluides de Toulouse, avenue du Professeur Camille Soula, 31400 Toulouse, France

(Received 4 July 1994; in revised form 3 March 1995)

Abstract—Numerical simulations of drainage and drying at low capillary number are performed. Drainage is simulated by means of the standard invasion percolation algorithm. Simulations of drying are based on an invasion algorithm combining elements of the invasion percolation algorithm with the computation of the vapour flux at each elementary liquid–gas interface. The simulations show that the invasion front is the very same fractal object in drainage and in drying. Specific features of drying are investigated. It is shown that the evaporation front should be clearly distinguished from the invasion front. In the presence of gravity forces, the disconnected cluster erosion mechanism is very effective and no disconnected cluster can survive outside the invasion front region. In the absence of gravity forces, the simulations indicate that drying of an initially saturated capillary-porous medium cannot be described according to the continuum approach to porous media.

Key Words: porous media, drying, invasion percolation, gradient percolation, microscopic simulator

1. INTRODUCTION

Invasion percolation models, Wilkinson & Willemsen (1983), Chandler *et al.* (1982), Lenormand *et al.* (1988), Furuberg *et al.* (1988) to quote only a few representative references, have been used extensively to simulate slow drainage processes in a porous medium, i.e. the slow displacement of a wetting fluid by a non-wetting fluid in a porous medium. Experimental studies (Masmoudi *et al.* 1992), as well as numerical simulations (Prat 1993), have shown that drying of initially saturated porous media may also be analysed to a certain extent in terms of invasion percolation. As shown in Prat (1993), however, drying presents some specific aspects that lead one to consider a modified form of invasion percolation, the main features of which are briefly recalled in section 3. Under these circumstances, the purpose of this paper is to study more precisely the main similarities and differences between drainage at low capillary numbers and drying. In fact, throughout this paper, results obtained for drainage at low capillary numbers serve as references to which results for drying are compared. At this stage, it should be noticed that in the classic continuum approach to drying in porous media [see Whitaker (1977) for example] the modelling of the liquid-phase flow in terms of generalized Darcy's law and relative permeability concept is basically analogous to the macroscopic modelling of drainage. Thus it is clearly of interest to investigate the analogy between drainage and drying. We also describe features of drying which are specific to drying. In this paper, however, the study is restricted to two-dimensional processes. We are aware that significant differences exist between three-dimensional and two-dimensional invasion percolation, mainly because of the trapping phenomenon of the wetting phase which is important in two dimensions and almost negligible in three dimensions. Nevertheless, much insight may be gained from two-dimensional simulations. Also, we assume an isothermal process. Naturally, drying is never a truly isothermal process since evaporating the liquid cannot occur without transfer of energy. However, we believe that the main features of the phase distribution evolution, that are described in this paper, are not significantly affected when small temperature gradients are present (as in the case of drying at low drying rate). Clearly, the emphasis here is on the understanding of the fluid transport mechanisms occurring within the pore spaces during drying and their relation to drainage. Our study applies to non-hygroscopic capillary-porous materials [see Keey (1972)] and

is, in fact, of interest not only to drying but also to certain light oil vaporization processes occurring in a fractured reservoir (Morel *et al.* 1990).

2. DRAINAGE AS AN INVASION PERCOLATION PROCESS

Drainage in a porous medium has been extensively studied. In the absence of gravity forces, Lenormand (1985) has proposed a phase diagram mapping the various drainage regimes in terms of a capillary number Ca, which is the ratio of viscous forces to capillary forces, and the ratio M of the displacing fluid viscosity to the displaced fluid viscosity. As shown experimentally and numerically (Lenormand *et al.* 1988), three main regimes can be distinguished depending on whether capillary or viscous forces dominate. The regime associated with very low capillary numbers is termed capillary fingering and can be simulated by means of the standard invasion percolation algorithm. As drying is generally a very slow process associated with very low capillary numbers, we only consider drainage in the limit of very small capillary numbers. Physically, this means that the viscosity plays no role and that the drainage process is entirely controlled by the capillary forces. Hydrostatic equilibrium is, in fact, assumed at each step of the invasion process. In the absence of gravity forces, this means that the pressure is uniform and constant in each fluid phase. Naturally, there exists a pressure jump, the capillary pressure, between the pressures of each fluid phase. Gravity effects, however, are present in most cases since the two fluids very often have significantly different densities. This is especially true in drying since in drying the liquid phase, typically water, is 1000 times as dense as the gas phase, typically air, under standard conditions. Wilkinson (1984) has proposed a method, based on the assumption of quasi-static equilibrium between the gravity forces and the capillary forces, for simulating the gravity effects by means of the invasion percolation algorithm. The validity of Wilkinson's approach has been demonstrated in two dimensions by the simulations and experiments of Birovljev *et al.* (1991) and in three dimensions by the experiments of Clément *et al.* (1985, 1987) and Hulin *et al.* (1988). In this approach, the porous medium is modelled by a square lattice of size $L \times L$ consisting of nodes (pores) and bonds (throats). The width l of the bonds is randomly chosen according to a given distribution law (a uniform distribution is used in the present paper). As the capillary pressure associated with each throat is inversely proportional to l, l^{-1} represents the threshold value for the normalized capillary pressure needed to invade the throat connecting two pores. When the gravity forces are taken into account, an invasion potential Q depending on l, the hydrostatic pressure gradient and the throat's position z measured from the top edge of the lattice is assigned to each throat. One may define this potential as

$$Q = -\frac{\sigma}{l}\left(1 - \mathrm{B}\frac{l(L-z)}{a^2}\right) + \text{const.} \qquad [1]$$

where B, which can be thought of as a dimensionless hydrostatic pressure gradient, is the Bond number which accounts for the competition between capillary and gravity forces,

$$\mathrm{B} = \frac{\Delta\rho g a^2}{\gamma} \qquad [2]$$

in which a is the distance between two nodes of the network and γ is the interfacial tension. To simulate drainage, the network is assumed to be initially fully saturated by the wetting fluid. The non-wetting fluid enters through the top edge of the network. The wetting fluid escapes through the bottom edge of the network (figure 1). At each step the pore which is invaded is the one which is connected to the region already invaded by the throat that has the lowest potential. Because of the incompressibility of the displaced fluid, regions which become surrounded by the invading fluid cannot be invaded and are trapped. The process ends when the bottom edge is reached. This final stage of the invasion process is the breakthrough point (BT).

3. DRYING MICROSCOPIC SIMULATOR

As shown in Prat (1993), isothermal drying of non-hygroscopic capillary-porous materials can be simulated by combining elements of the standard invasion percolation algorithm with the

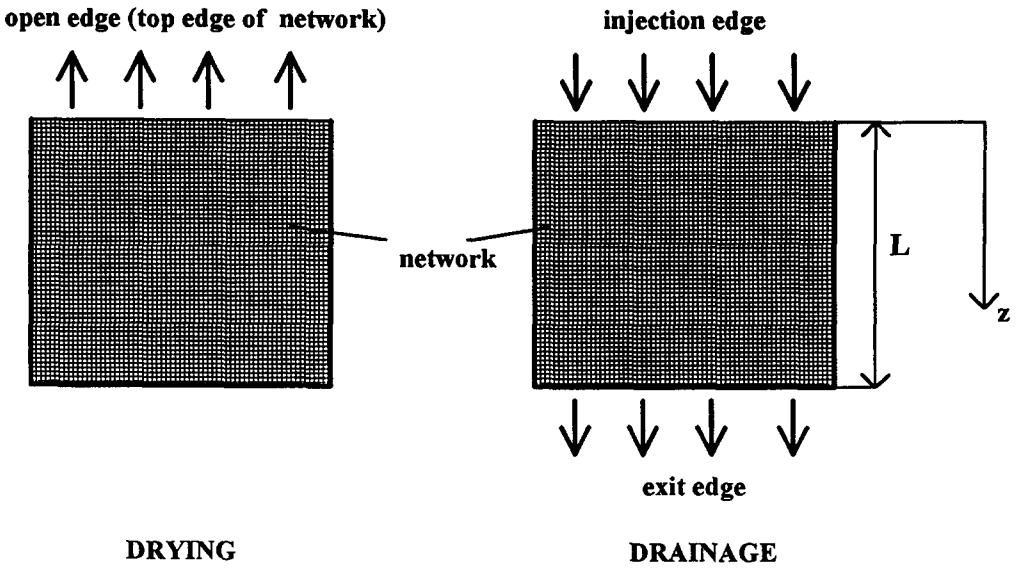

Figure 1. Schematic of drying and drainage of a 2-D network.

computation of the binary diffusion of the vaporized species in the gas phase, which is assumed to be made up of the vapour of the liquid and an inert component, and the evaporation flux at each elementary liquid–gas interface. As in the standard invasion percolation algorithm, an invasion potential is assigned to each throat according to [1]. The gas-phase diffusion computation is performed at each invasion step by expressing the mass flux balance at each node occupied by the gaseous phase under the following assumptions [see Prat (1993) for more details]

—the diffusion process is quasi steady
—at each elementary liquid–gas interface, local thermodynamic equilibrium is assumed (the Kelvin effect is, however, neglected)
—liquid films, if any, along the walls of the pores or throats occupied by the gaseous phase are not taken into account
—one-dimensional transport by diffusion is assumed in each throat occupied by the gas phase.

As for the drainage case, the network is initially completely saturated by liquid. At the top edge of the network, a uniform and constant local mass transfer coefficient is used to compute the flux of the vaporized species. Zero flux conditions are imposed at the lateral and bottom edges of the network. The vaporized species escapes through the top edge of the network (figure 1). The simulation of drying is based on the following procedure: (1) every cluster present in the network is identified; (2) the throat connected to the already invaded region which has the lowest potential is identified for each cluster; (3) the concentration of the vaporized species is determined at each node occupied by the gaseous phase; (4) the evaporation flux at the boundary of each cluster is computed; (5) for each cluster, the mass loss during an elementary time step is computed and is used for computing the emptying of the throat selected in (2); (6) the throat among the throats selected in (2) which empties the first is declared invaded as well as the adjacent pore; and (7) the phase distribution within the network is updated and the above-described procedure is repeated. Contrary to standard invasion percolation, the regions which become surrounded by the invading fluid can be invaded. The process ends when the network is completely occupied by the invading fluid.

4. SIMILARITIES BETWEEN DRYING AND DRAINAGE AT LOW Ca

4.1. Invasion front and drying front

Low evaporation rate drying fronts have been observed in a number of experimental studies (Maneval *et al.* 1991; Masmoudi *et al.* 1992; Shaw 1987 among others). They resemble the drainage

fronts at low capillary numbers observed experimentally, notably by Lenormand *et al.* (1988), Clément *et al.* (1985, 1987) and Birovljev *et al.* (1991). In this section, we show that the invasion front obtained by means of the standard invasion percolation algorithm, which simulates drainage at low capillary numbers, and the drying front obtained by means of the simulator described in section 3 are identical. The remainder of the section is devoted to a recall of the main results which have been obtained on two-dimensional invasion fronts in drainage which are also relevant to drying fronts. The front is defined as the external frontier of the invading fluid cluster which is in contact with the wetting phase. The front is one part of the liquid–gas interface within the system. The other part consists of the frontier of the disconnected wetting fluid clusters, i.e. the liquid clusters which are not connected to the bottom edge of the network shown in figure 2. Thus, if, at a given step, all the liquid disconnected clusters were replaced by gas, the gas–liquid interface would be made of all the sites belonging to the front. More specifically, the front is made of the sites occupied by the non-wetting fluid and which have at least one liquid neighbour which does not belong to a disconnected liquid cluster. The front is shown in figure 3 at different stages of the drying process. In figure 3, the drainage front, obtained by means of the ordinary invasion percolation algorithm, is also shown at stages of the drainage process corresponding to the very same number of invaded bonds in the main wetting fluid as in the simulation of drying [the "main" cluster is the region occupied by the wetting fluid which is connected to the bottom edge of the network. It is convenient to distinguish the main cluster from the disconnected clusters, i.e. the clusters completely surrounded by the invading fluid (figure 2)]. In both cases, i.e. drainage and drying, the same 100×100 network was considered. No gravity forces, i.e. $B = 0$, are taken into account in these simulations. Figure 3 clearly shows that the drainage front and the drying front are the very same object. This is not surprising and, in fact, is fully consistent with the drying algorithm presented in section 3. As far as the main liquid cluster is concerned, the selection procedure of the successive bonds and sites invaded in the main liquid cluster is identical in ordinary invasion percolation and in the drying algorithm. In other words, the sequence of the bonds and sites successively invaded in the main clusters is clearly independent of the fact that, contrary to ordinary invasion percolation, the disconnected liquid clusters are invaded and possibly dry up during the process. Naturally, this similarity between the drying front and the drainage front only holds up to the breakthrough point, i.e. when the gas phase reaches the bottom edge of the network. In two-dimensional ordinary invasion percolation, the invasion process stops at breakthrough. In drying, the invasion process may continue up to a complete dry-out of the network. In drying also, the first time the gaseous phase reaches the bottom edge of the network may be termed

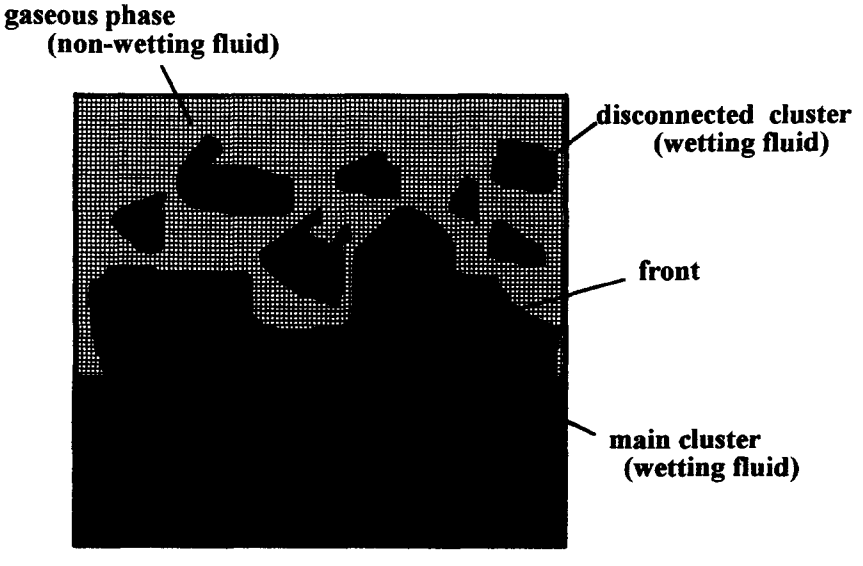

Figure 2. Schematic picture of the phase distribution within the network in terms of main cluster, disconnected clusters and front.

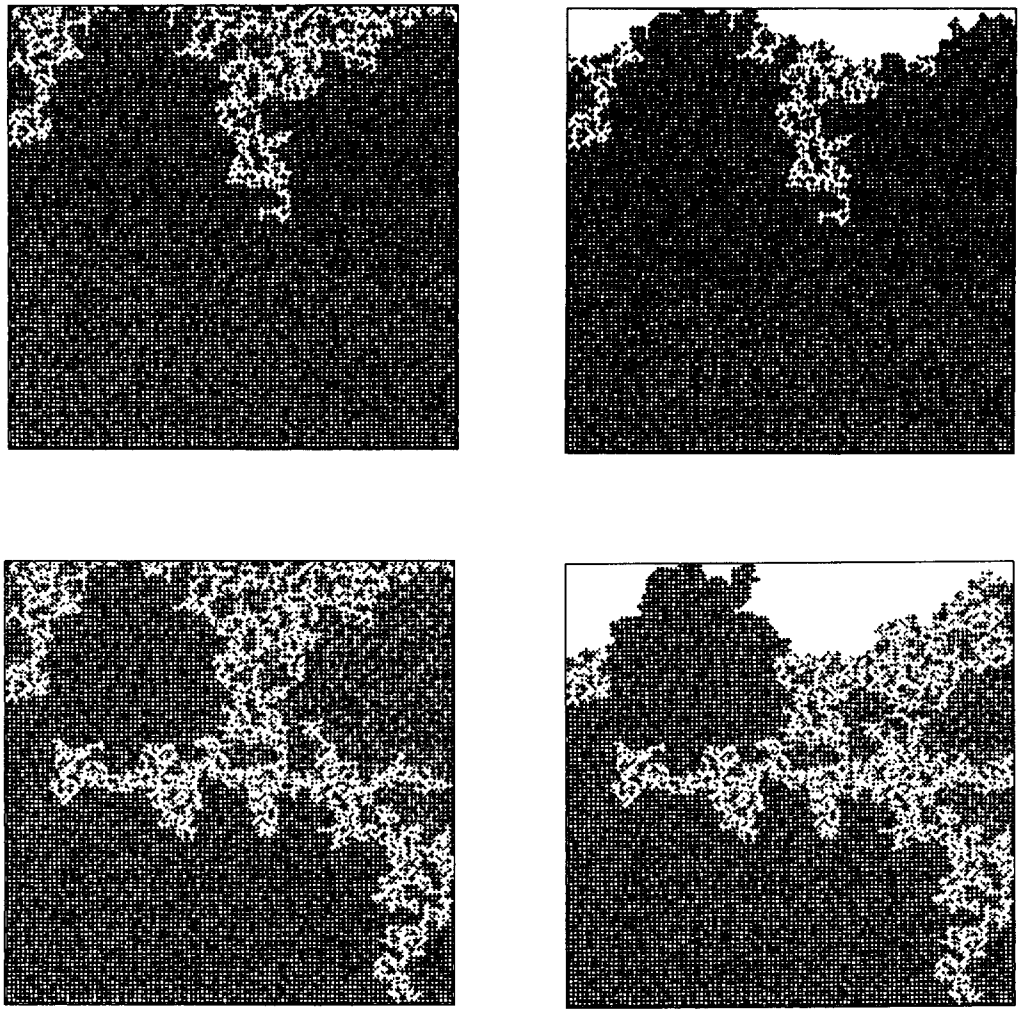

Figure 3. Phase distributions at breakthrough in drainage and in drying for the same realization of the network for B = 0. The disconnected clusters are in grey, the clusters connected to the exit side in black, the non-wetting fluid and the solid phase in white. The front forms the frontier between the regions in black and the region occupied by the non-wetting fluid.

breakthrough. Hence we will, for convenience, distinguish a first drying phase up to breakthrough from a second drying phase which takes place after breakthrough. The first drying phase presents many similarities with drainage at low Ca. The second phase is specific to drying and is discussed in section 5.3. The results presented in figure 3 correspond to B = 0. However, it is clear that the drying front and the drainage front are the same object not only for B = 0 but also in the presence of the gravity forces, as shown in figure 4. As discussed above, the sequence of selected bonds in the main cluster is independent of the fact that secondary invasions take place in the disconnected clusters in drying. Thus, for a given network and for the same Bond number, this sequence must be identical according to the drying algorithm or the ordinary invasion percolation algorithm. This allows us to take advantage of the numerous results concerning the invasion front under gravity. Indeed, gravity invasion fronts in porous media have been extensively studied within the framework of the gradient percolation model introduced by Sapoval *et al.* (1985) for the completely different case of diffusion front. The validity of the gradient percolation model has been verified experimentally through the three-dimensional experiments of Clément *et al.* (1985, 1987, 1988).

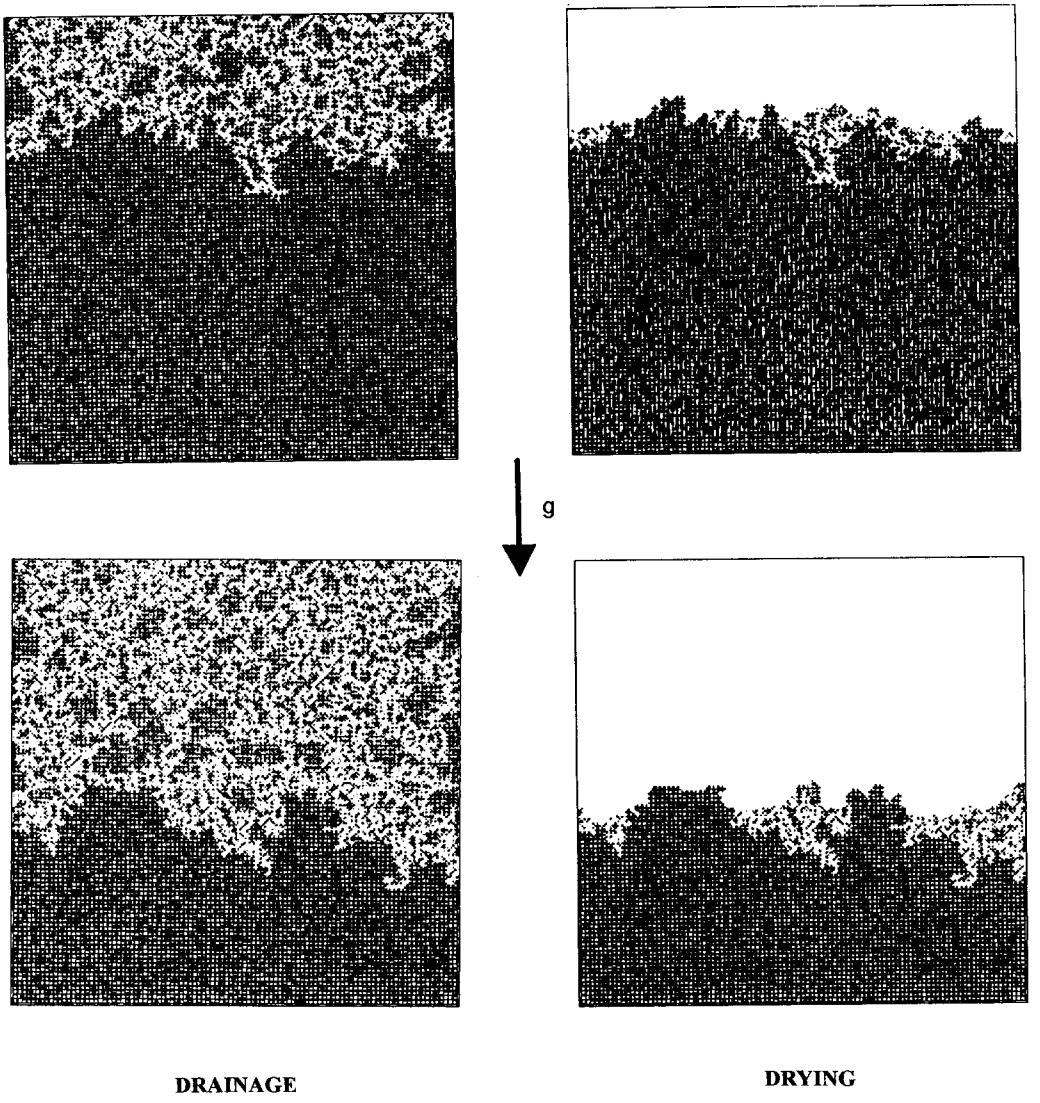

Figure 4. Phase distributions in the presence of gravity forces in drainage and in drying for the same realization of the network. The disconnected clusters are in grey, the clusters connected to the exit side in black, the non-wetting fluid and the solid phase in white. The front forms the frontier between the regions in black and the region occupied by the non-wetting fluid.

However, only one value of B was used in these experiments. Furthermore, the structure of the front in three dimensions is quite different from the two-dimensional structure which is of interest for the present study. More recently, Birovljev *et al.* (1991) performed slow drainage experiments as well as computer simulations in the two-dimensional case over a range of B. Their results on the width σ of the front and the fractal dimension of the front are in very good agreement with the gradient percolation approach. According to these various studies the front is a fractal object. Its fractal dimension, as measured by Birovljev *et al.* (1991), is $D_{exp} \approx 1.34$ and is consistent with the fractal dimension of the external perimeter of the percolation cluster, $D_e \approx 1.37$ (Stauffer & Aharony 1992). In agreement with the theoretical prediction of Sapoval *et al.* the experimental and numerical results of Birovljev *et al.* (1991) are consistent with the following scaling law

$$\sigma \propto B^{-\nu/(1+\nu)} \qquad [3]$$

where ν is the correlation length critical exponent (Stauffer & Aharony 1992), $\nu = 4/3$ in two dimensions. In [3], σ is the width of the front which is defined as

$$\sigma^2 = \frac{\int_0^\infty (z_f - z)^2 p_f(z)\, dz}{\int_0^\infty p_f(z)\, dz} \quad [4]$$

where z_f is the mean position of the front,

$$z_f = \frac{\int_0^\infty z p_f(z)\, dz}{\int_0^\infty p_f(z)\, dz} \quad [5]$$

$p_f(z)$ is the probability of finding one site of the front at z (i.e. the number of sites located at the distance z from the top edge of the system and belonging to the front divided by the total number of sites). As already noted in Prat (1993) and as is made clear by [3], the effect of gravity is to stabilize the drying front. The drying front has a finite width resulting from the equilibrium between the capillary forces and the gravity forces. On the contrary, in the absence of gravity forces, there is no characteristic length scale. The front may span the whole network at breakthrough as is shown in figure 3.

4.2. *Clusters*

As explained above, the sequence of invaded bonds and sites in the main cluster is identical in drying and in drainage (for a given network, a given B and low Ca). It follows that the disconnected

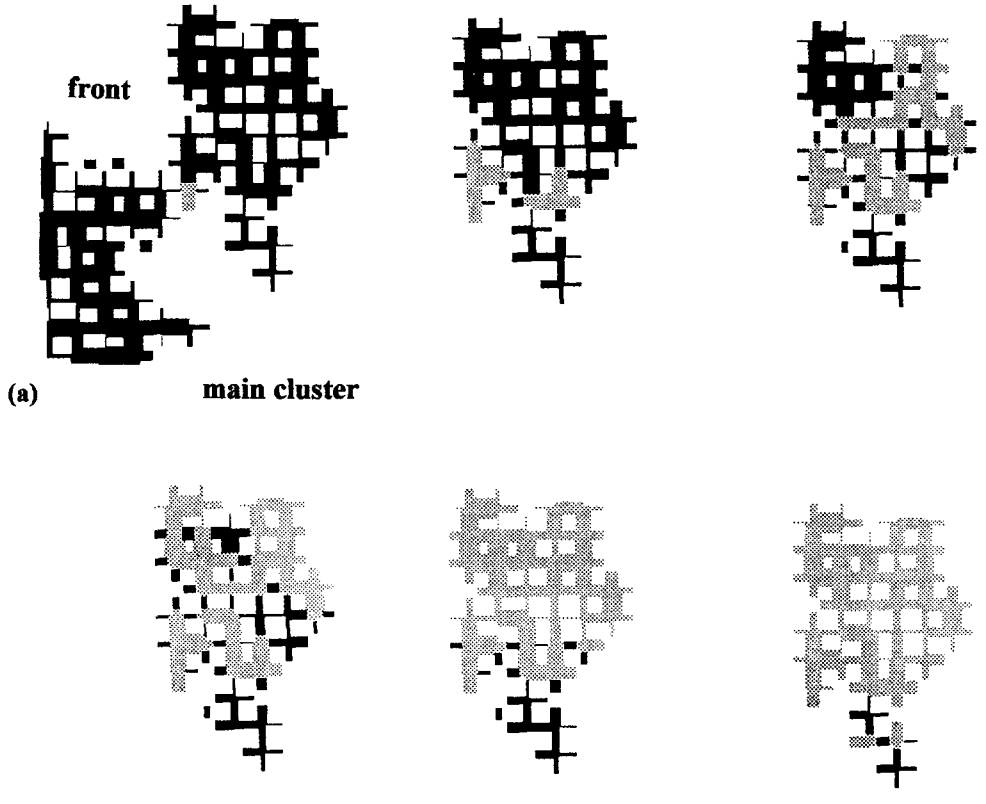

Figure 5. Birth of a cluster from the main cluster when the bond and the adjacent site in grey in (a) are invaded and successive invasions of the cluster. The liquid phase is in black and the invaded bonds and sites are in grey.

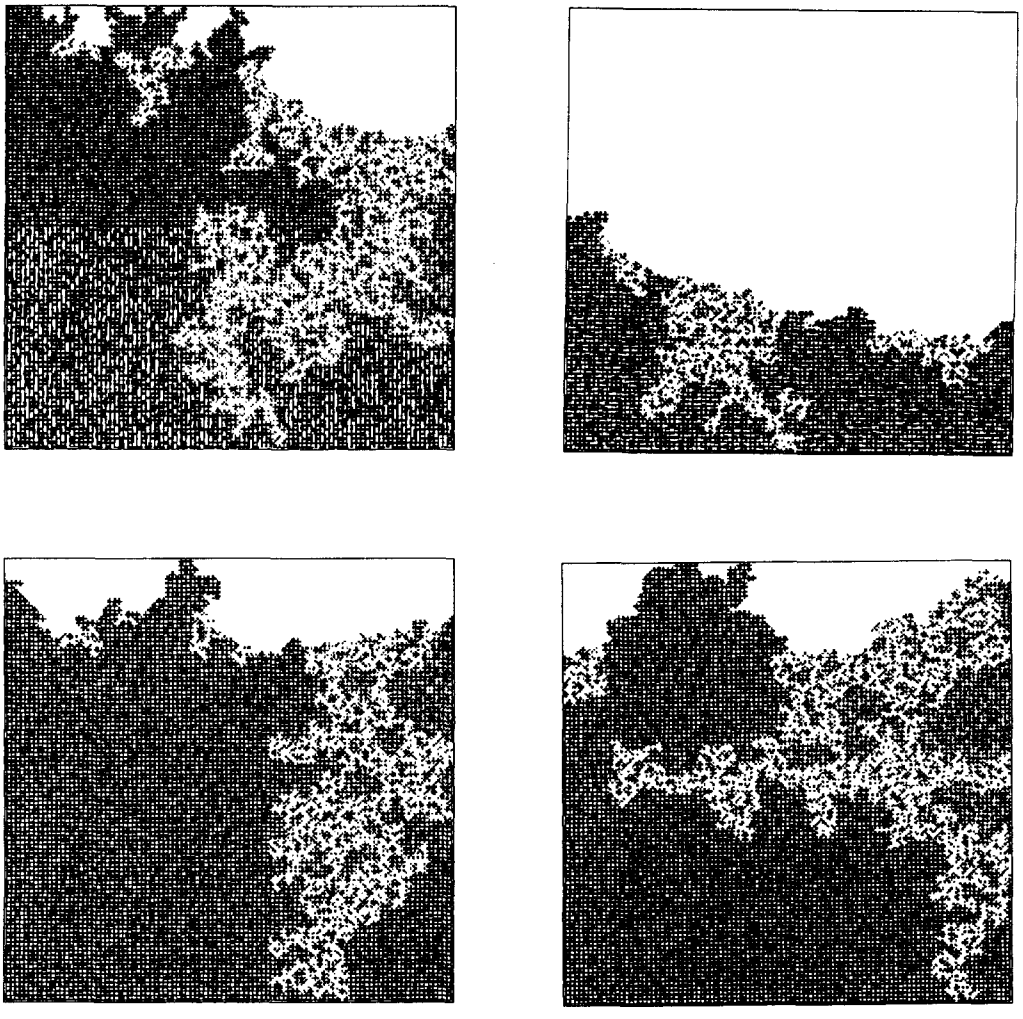

Figure 6. Phase distributions at breakthrough in drying for four different realizations of a 100×100 network.

clusters formed in drying and in drainage are identical since a disconnected cluster is, in fact, a part of the front which gets disconnected from the front at some stage of the invasion process as is illustrated in figure 5. Naturally, once a cluster has been disconnected from the front, it is trapped for good in drainage because of the incompressibility of the fluid. In drying, evaporation takes place at the boundary of the disconnected clusters and therefore they eventually disappear through the action of evaporation. Thus the birth of the disconnected clusters is identical in drainage and drying but their life is completely different. This is clearly shown in figure 3 where some of the clusters visible in the top edge region in drainage have disappeared in drying. Again, the fact that the birth of the disconnected clusters is identical in drying and drainage only holds up to the breakthrough. At breakthrough, invasion of the liquid stops in drainage but continues in drying. In the absence of gravity forces, clusters of an arbitrary large size are created. In the presence of gravity forces, the cluster size cannot exceed a certain size since equilibrium between the capillary and gravity forces must be enforced. Wilkinson (1984) has shown that the size of the largest clusters scales as

$$L_{\max} \propto \mathbf{B}^{-\nu/(1+\nu)} \qquad [6]$$

It is worth noting that this scaling is fully consistent with the front thickness scaling ([3]). Clearly, since a cluster is basically a part of the invading front which becomes disconnected, the size of the

largest clusters should be of the order of the deepest "fjords" of the front, i.e. of the order of the front thickness σ.

5. DIFFERENCES BETWEEN DRYING AND DRAINAGE AT LOW Ca

5.1. Cluster erosion mechanism

As discussed above, before reaching breakthrough, the disconnected clusters being formed in drainage and in drying are initially identical (for a given porous structure). In drying, however, as evaporation takes place at the boundary of the cluster secondary invasions occur and eventually the cluster disappears. Figure 5 shows the various stages of "life" of a cluster from birth to death. As can be seen from figure 5, secondary invasion of a cluster generally gives birth to two clusters of smaller size, these two clusters are then invaded and each gives birth to two smaller still clusters. This process continues until the clusters being formed evaporate without giving birth to smaller clusters. As discussed in section 5.4 and shown in figure 4, the cluster erosion mechanism is much more effective in the presence of gravity forces. In the absence of gravity forces, one may wonder

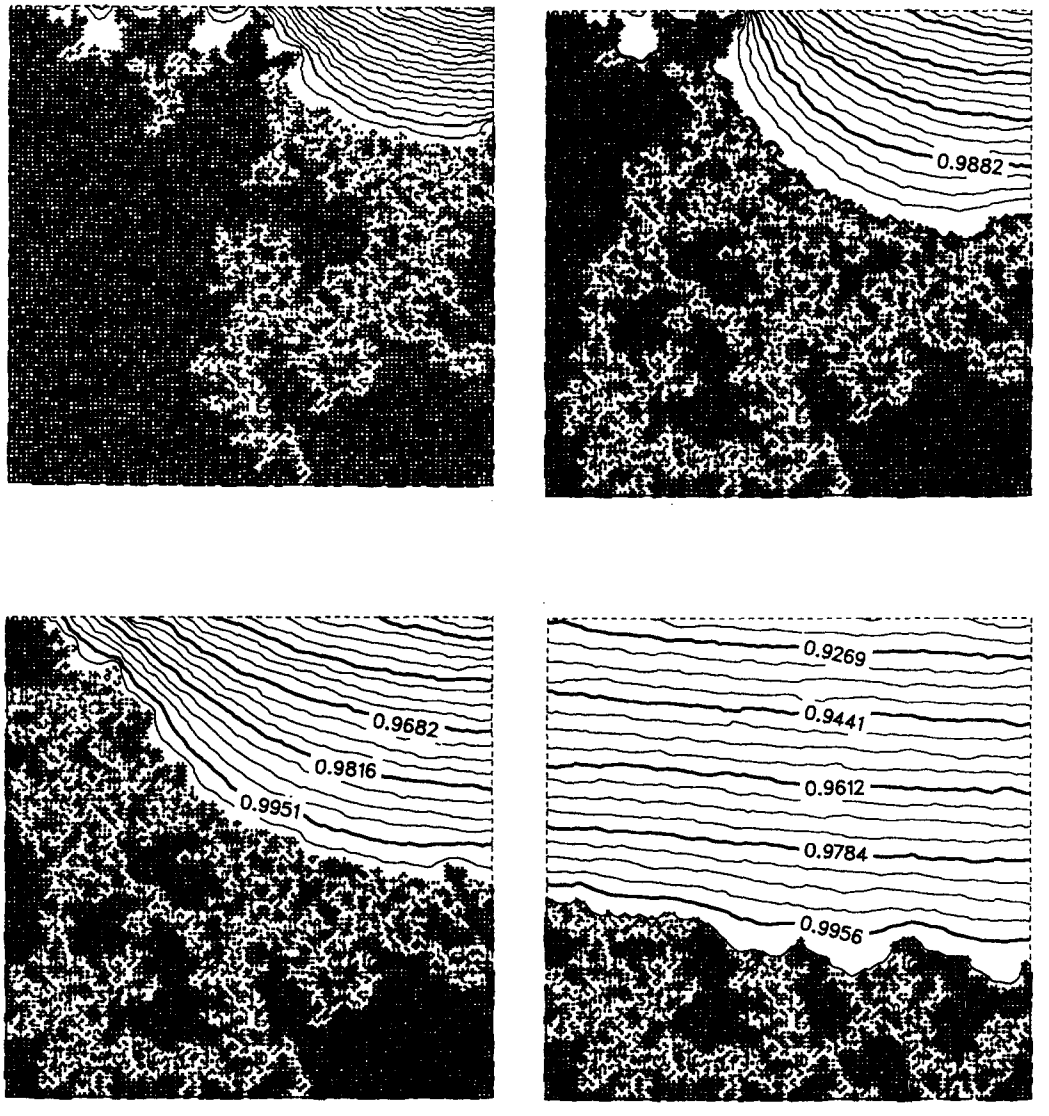

Figure 7. Phase distributions within the network at various stages of drying together with the vaporized species normalized gas concentration distribution within the gaseous phase (B = 0).

whether this elimination mechanism is significant before breakthrough. As can be seen from figure 6, various situations may be encountered depending on the realization of the network.

5.2. Invasion front and evaporation front

As discussed in section 4.1, the drying front and the drainage front are the very same fractal object and may be termed the invasion front. The invasion front, however, should be clearly distinguished from the evaporation front, i.e. the frontier between the cluster region and the dry zone where the diffusive transport in the gas phase becomes important. To visualize the evaporation front, the vaporized species normalized gas phase concentration distribution is shown in figure 7 as well as the phase distribution at various stages of drying. As can be seen from figure 7, the concentration is quasi-uniform and very close to the equilibrium concentration at the liquid–gas interfaces within the cluster zone. This indicates that the vaporized species diffusive transport in the gas phase is almost zero within the cluster zone. Figure 7 shows that the evaporation front roughly forms the upper boundary of the cluster zone. To further characterize the evaporation front, one considers the sites occupied by the gaseous phase and such that all first neighbour sites are occupied by the gaseous phase (those sites are such that each of their connecting throats to the neighbour sites are occupied by gas). As illustrated in figure 8, this type of site may be encountered within the cluster regions where they are isolated and scattered. In fact, they are essentially encountered in the gaseous zone where they form a well identified region of neighbouring sites. The evaporation front forms the lower boundary of this region.

5.3. Drying after breakthrough (in the absence of gravity forces)

What happens after breakthrough is specific to drying since invasion of the wetting phase stops at breakthrough in drainage. In the absence of gravity forces, there are generally in the network two very large clusters born of the main cluster and a family of smaller clusters of various size at breakthrough, as shown in figure 6. Then subsequent invasions of the clusters take place. In agreement with the erosion mechanism described in section 5.1 the clusters present in the system

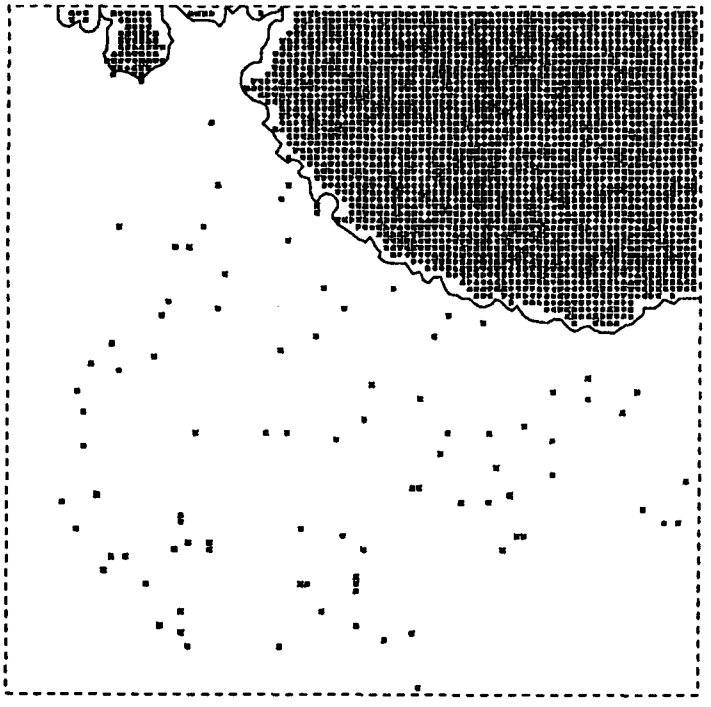

Figure 8. Geometric definition of the evaporation front in terms of the frontier of the region containing the gaseous sites having four gaseous first neighbour sites. The isoconcentration line corresponding to the equilibrium concentration in the gas phase is also shown (see also figure 7).

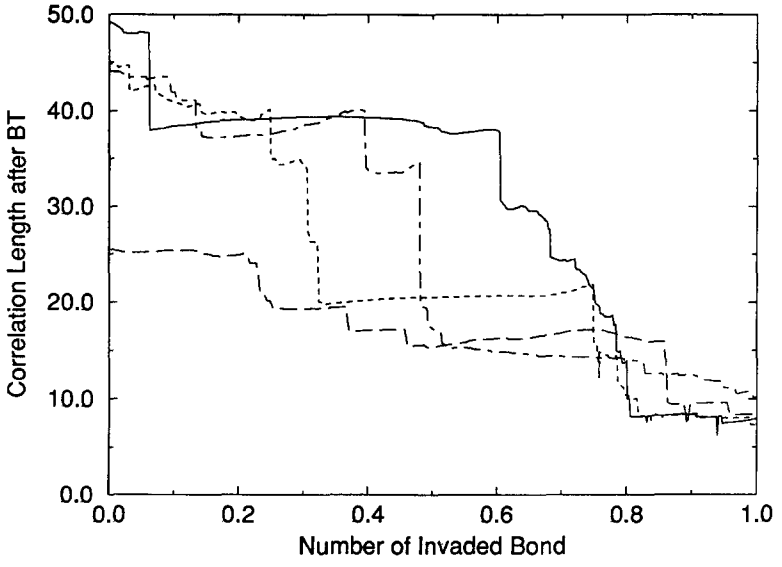

Figure 9. Drying after BT (B = 0). Correlation length, expressed in network units (distance between two sites), of the liquid clusters as a function of the normalized number of invaded bonds for four different realizations of a 100 × 100 network.

become smaller and smaller and are progressively eliminated by evaporation. This is clearly shown in figures 9 and 10 where the correlation length and the average clusters size [see Stauffer & Aharony (1992) for definitions] are plotted as a function of the normalized number of invaded bonds after breakthrough for 4 realizations of a 100 × 100 network (the normalized number N of invaded bond is defined as $N = (n - n_{BT})/(n_{tot} - n_{BT})$ where n is the number of invaded bonds, n_{BT} is the number of invaded bonds at BR and n_{tot} the total number of bonds in the network). The evolution of the number of clusters present within the network after BT depends on two mechanisms: splitting of a cluster into smaller clusters and cluster elimination by evaporation. At some steps of the process, the successive splits of the clusters into smaller clusters exceed the loss of clusters by evaporation, leading to an increase of the number of clusters present in the system. At other times, the cluster elimination mechanism due to evaporation is preponderant and the

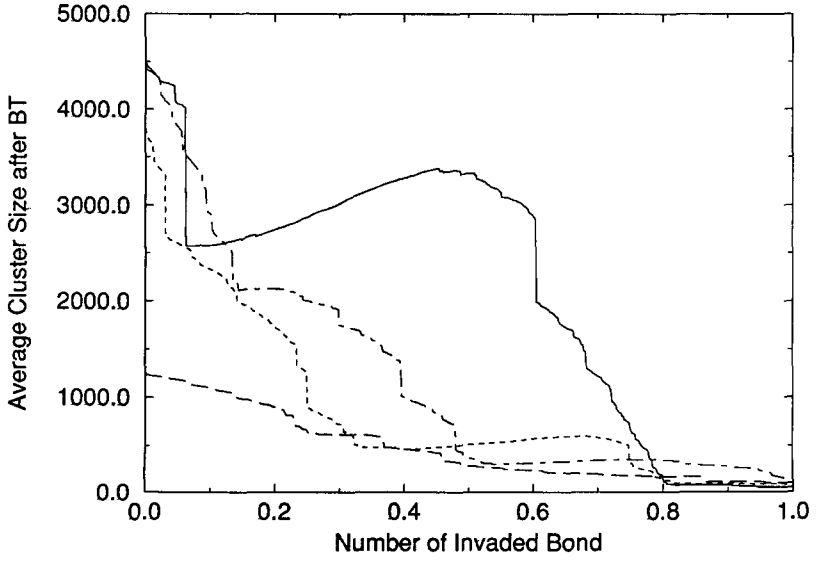

Figure 10. Drying after BT (B = 0). Average liquid cluster size, expressed in number of sites, as a function of the normalized number of invaded bonds for four different realizations of a 100 × 100 network.

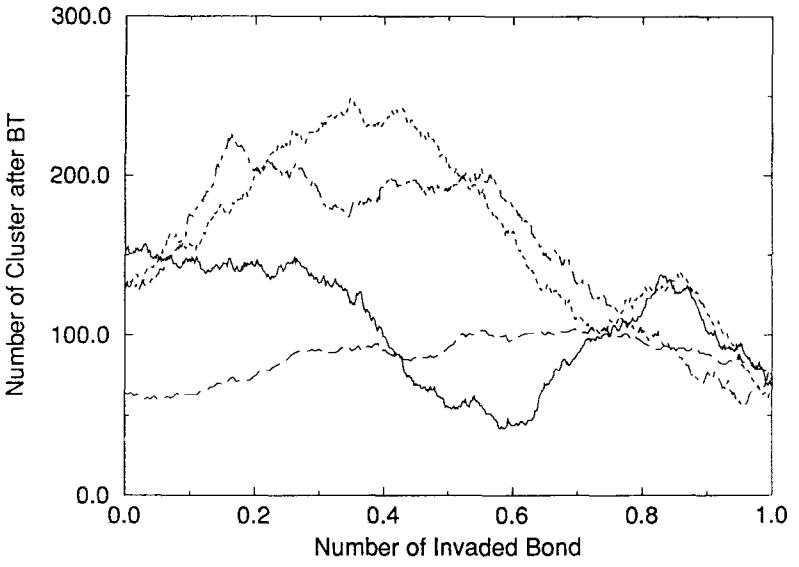

Figure 11. Drying after BT (B = 0). Number of clusters within the network as a function of the normalized number of invaded bonds for four different realizations of a 100 × 100 network.

number of clusters decreases as can be seen from figure 11. The fact that the clusters get smaller and smaller after BR as the non-wetting fluid saturation increases, i.e. the occupation probability increases after BT, is consistent with the percolation theory. Here, however, the occupation probability is not uniform since liquid is more likely to be stripped from the clusters located close to the top edge. Thus the occupation probability is greater in the top region of the network. In other terms, a dry zone progressively develops from the top edge as can be seen from figure 7.

5.4. Drying in the presence of gravity forces

As explained in section 4.1, taking into account the gravity forces introduces a length scale resulting from the equilibrium between the capillary forces and the gravity forces. In this section we assume that this length scale, which one may consider to be the front width σ defined by [4], is small relative to the size of the system, $\sigma < L$. Under these circumstances, one observes a well defined region of finite vertical extension, of width σ, containing the invasion front and most of the disconnected clusters (figures 4 and 13). One striking feature of drying in the presence of gravity forces is that there is almost no disconnected cluster outside the invasion front region. The disconnected clusters are mainly located within the "fjords" of the invasion front. Consistently, the vaporized species gas-phase concentration is quasi-uniform within the disconnected cluster region and very close to the equilibrium concentration as can be seen from figure 12. As for the "no gravity" case discussed in section 5.2, the evaporation front should be distinguished from the invasion front. In our simulations, the evaporation front forms the upper boundary of the invasion front region as shown in figure 12. Figure 12 makes it clear that there is almost no evaporation at the boundary of the disconnected clusters located within the "fjords" away from the evaporation front. The evaporation taking place at the evaporation front is associated with disconnected clusters as well as the main cluster. Thus, the evaporation processes cause, on the one hand, the migration of the invasion front downwards, and on the other hand, the stripping of the disconnected clusters. These two processes, migration of the invasion front and erosion of the disconnected clusters, take place simultaneously in such a way that no disconnected cluster remains outside the invasion front region. According to the gradient percolation approach ([3]), the structure of the two-phase region, i.e. the invasion front region, is statistically independent of time and depends only on the Bond number. This means that, except for the early and the final stages of the process, quantities such as the number of disconnected clusters present within the two-phase zone, the width of the invasion front, the fraction of the invasion front and the fraction of the disconnected clusters concerned by evaporation, ... are statistically constant for a given Bond number. This is clearly evident by our

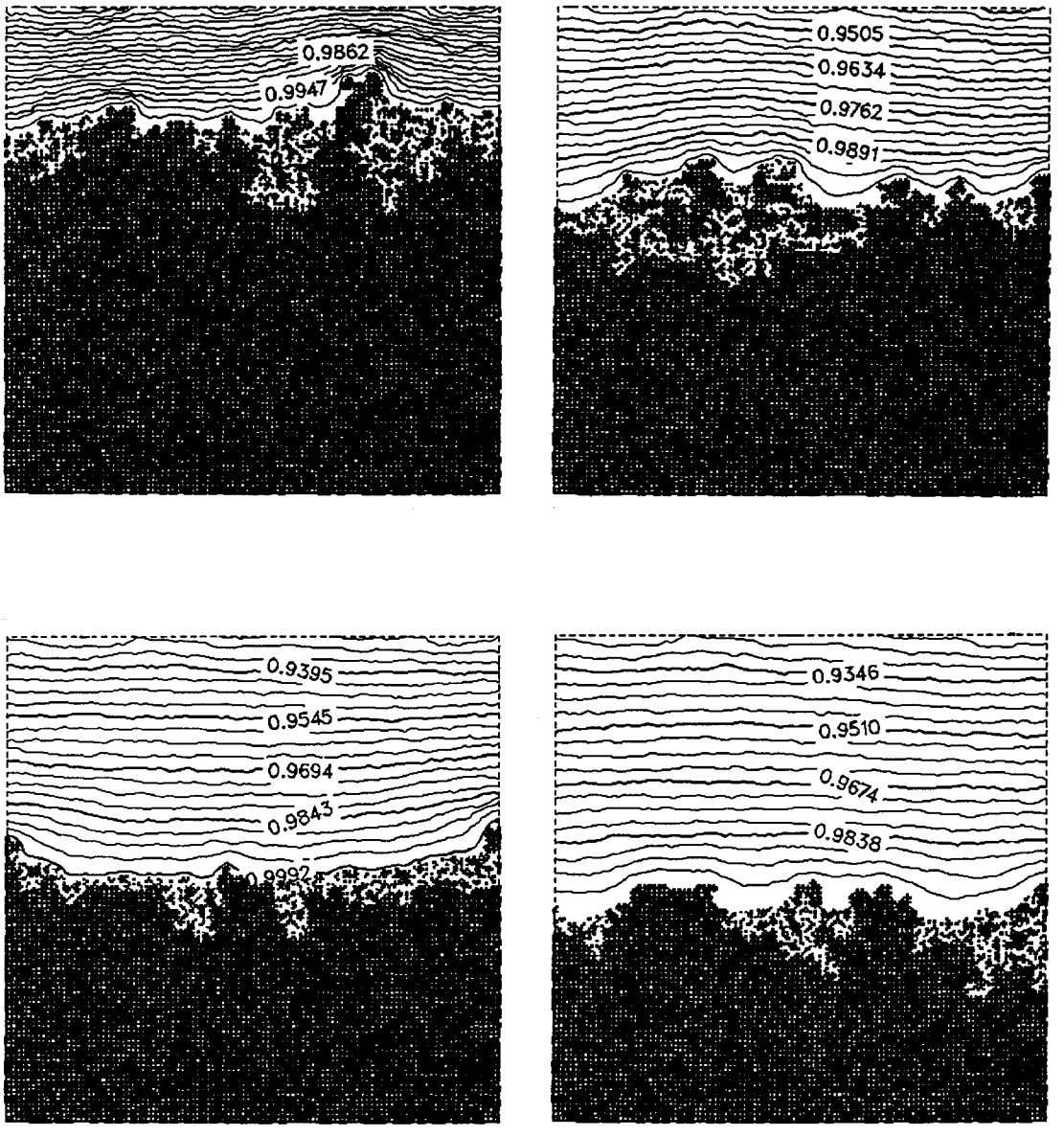

Figure 12. Phase distributions within the network in the presence of gravity forces at various stages of drying together with the vaporized species normalized gas concentration distribution within the gaseous phase.

simulation as can be seen from figures 13–16. Thus, for sufficiently large Bond numbers, there is a length scale separation between the thickness of the front and the size of the system. This indicates that, contrary to the no gravity or too small Bond number case, a macroscopic description is possible. In fact, for the simple geometry considered in this paper, the problem takes the form of a moving evaporation front problem analogous to the Stefan diffusion tube problem (Bird *et al.* 1960). This is evident in figure 17 which shows that the mean position of the front z_f is proportional to $\sqrt{t}$ (except in the very first phase of drying when the front is not yet established). Thus

$$z_f \propto \sqrt{t} \quad \text{when } \sigma \ll L \qquad [7]$$

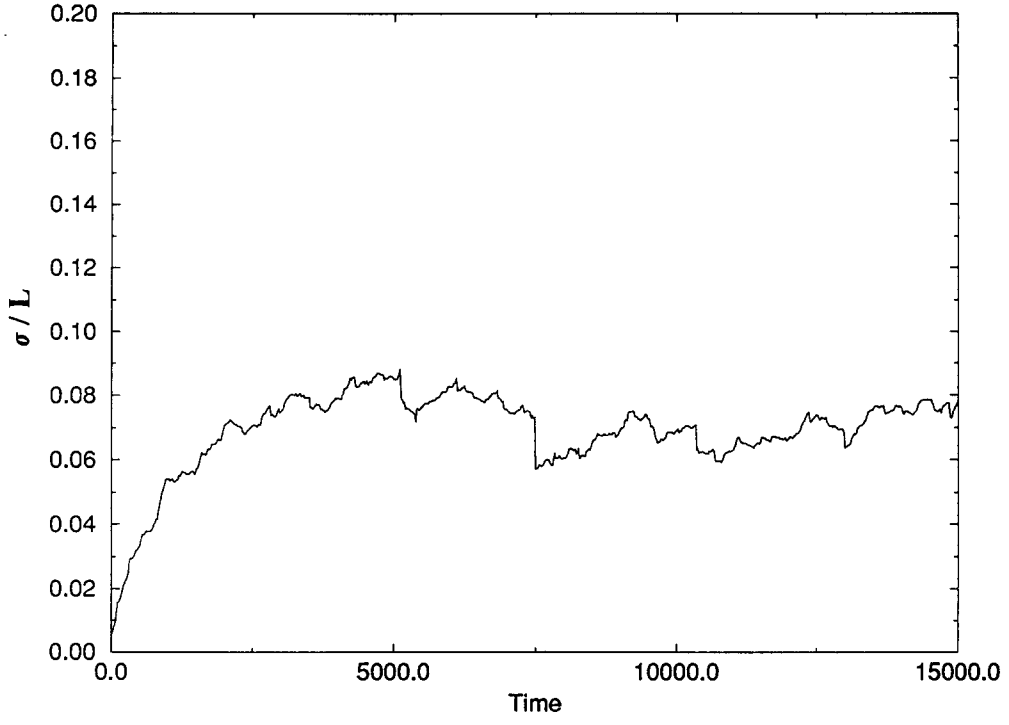

Figure 13. Drying for $B > 0$. Drying invasion front thickness, averaged over four realizations of a 100×100 network, as a function of the number of invaded bonds.

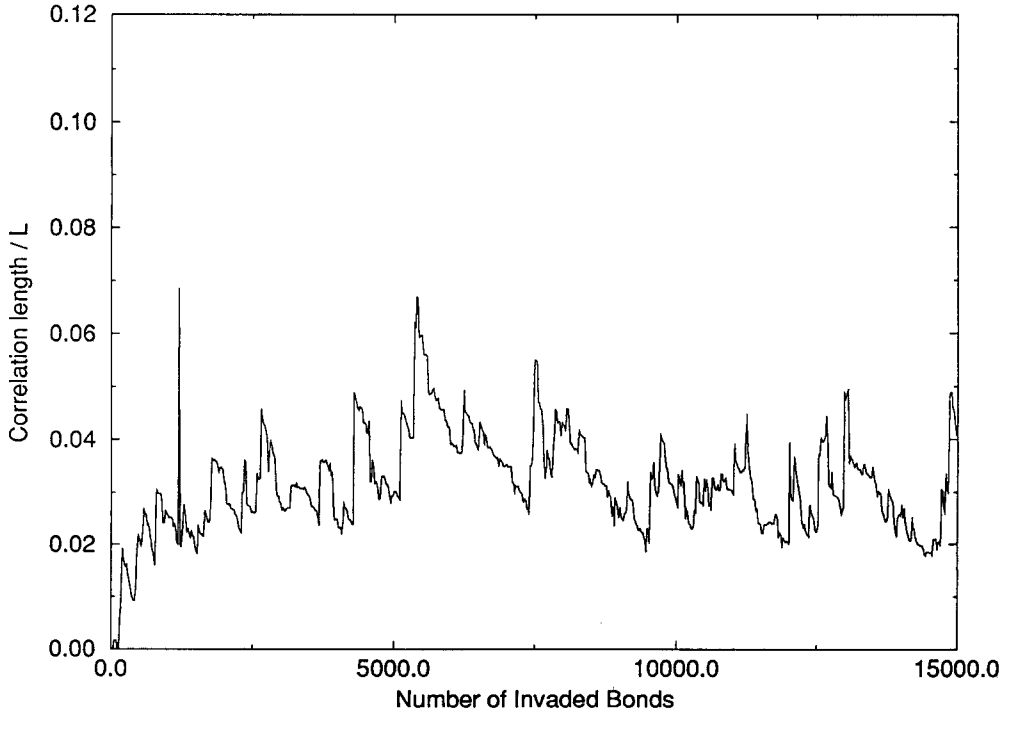

Figure 14. Drying for $B > 0$. Correlation length, averaged over four realizations of a 100×100 network, of the liquid clusters as a function of the number of invaded bonds.

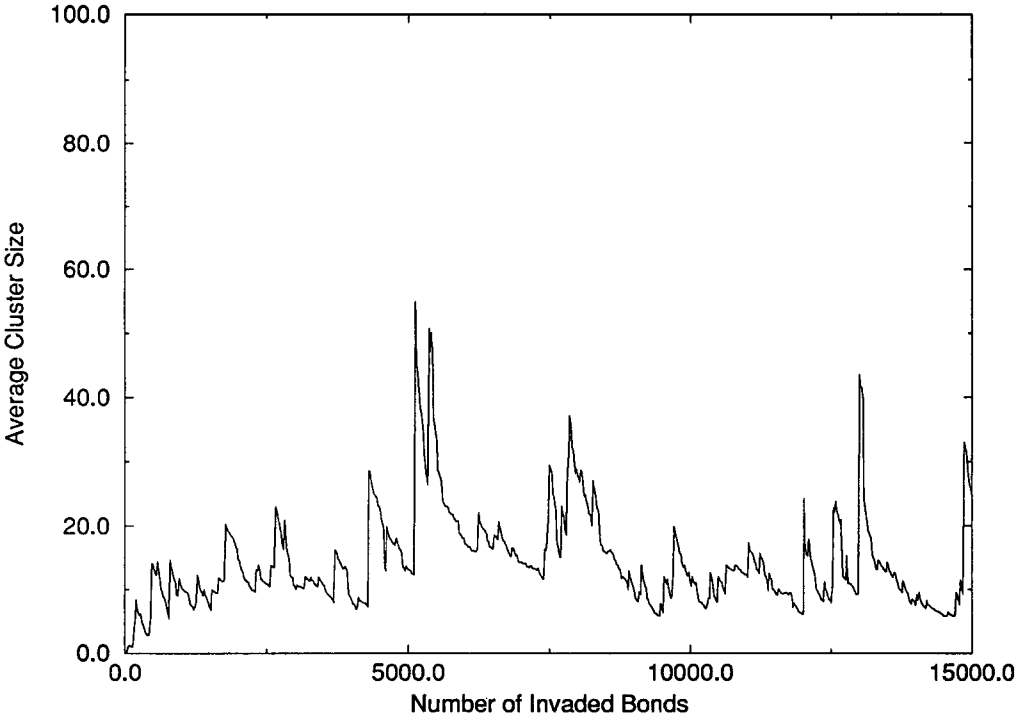

Figure 15. Drying for $B > 0$. Average liquid cluster size, expressed in number of sites and averaged over four realizations of a 100×100 network, as a function of the number of invaded bonds.

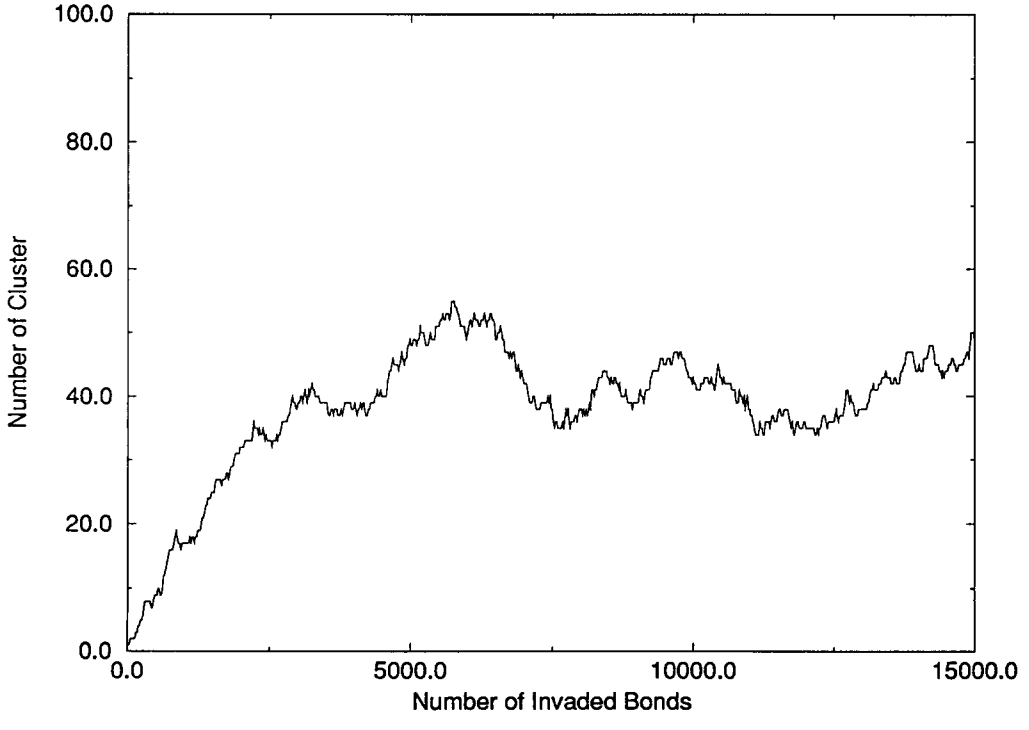

Figure 16. Drying for $B > 0$. Number of clusters, averaged over four realizations of a 100×100 network, within the network as a function of the number of invaded bonds.

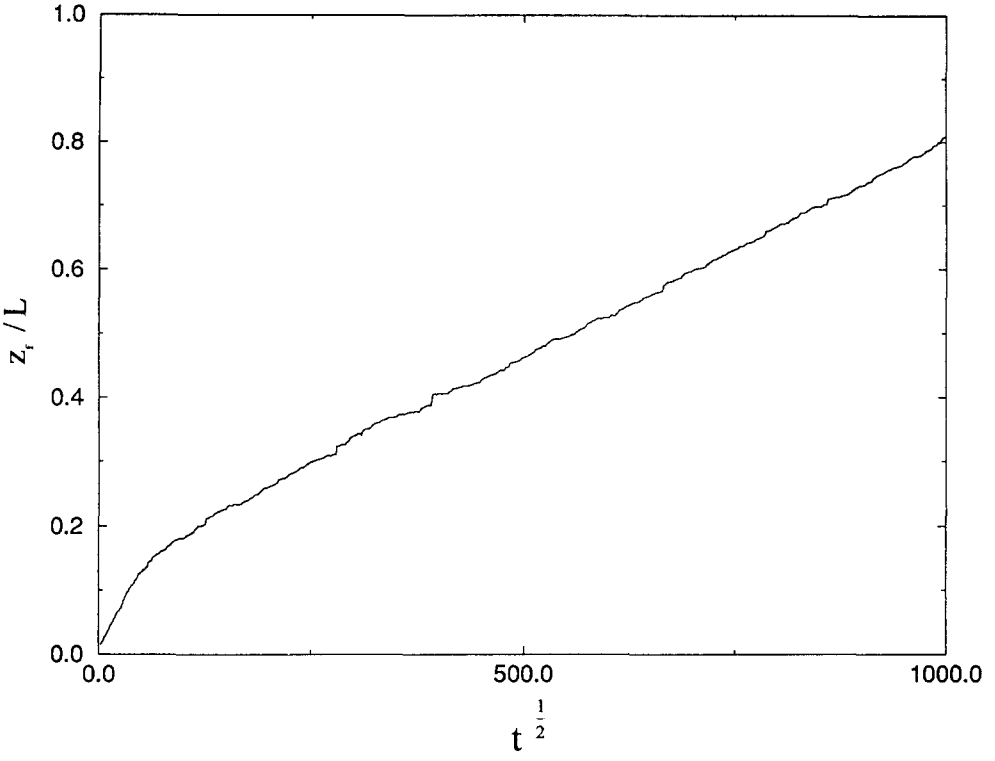

Figure 17. Time evolution of the mean position of the front, averaged over four realizations of a 100 × 100 network.

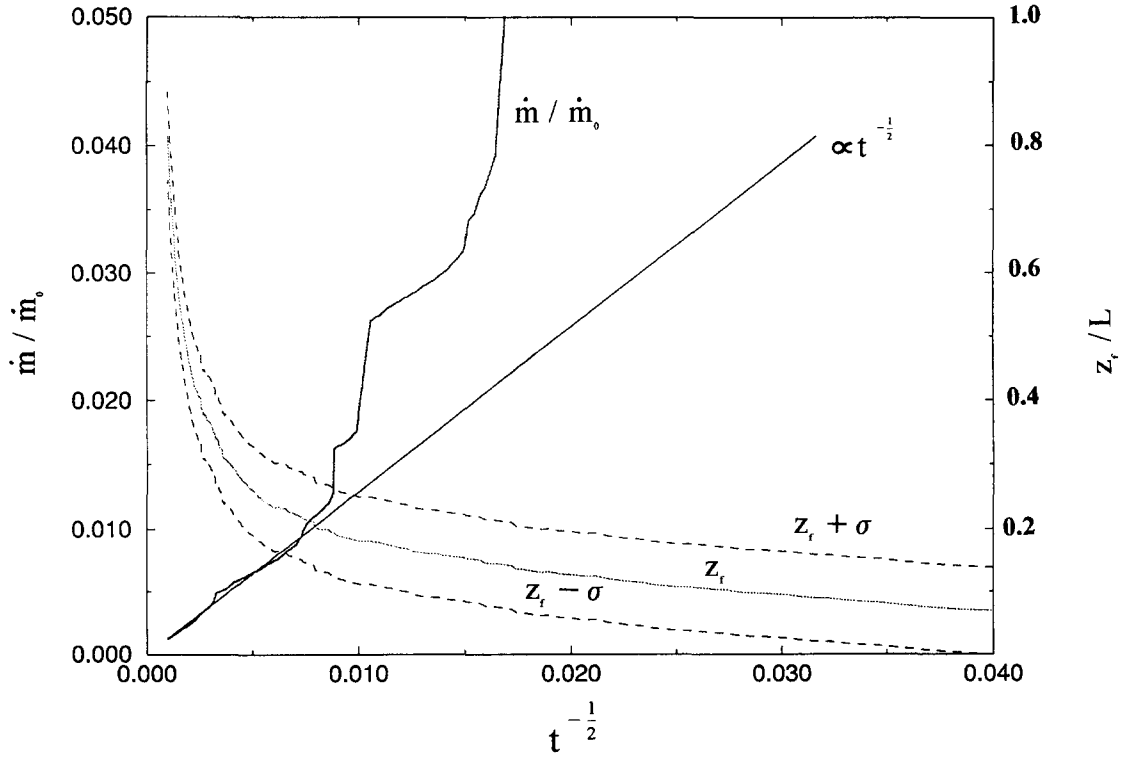

Figure 18. Time evolution of the drying rate $\dot{m}$ (normalized by the drying rate at $t = 0$), averaged over four realizations of a 100 × 100 network.

Also, as can be seen from figure 18, one observes that the drying rate $\dot{m}$, i.e. the evaporation flux at the interface, is proportional to $t^{-1/2}$, as for the Stefan diffusion tube, except naturally in the early stages of drying, i.e.

$$\dot{m} \propto t^{-1/2} \quad \text{for } \sigma \ll L \quad \text{and} \quad z_f > \sigma \qquad [8]$$

As shown in figure 18, however, important errors can be expected if a simple moving diffusion front model is used to predict the evaporation flux in the early stages of the process. Clearly, a specific study of this phase of drying is needed to develop a fully predictive model at the macroscopic level. This will be the subject of future work.

6. CONCLUSIONS

In this paper, similarities between drainage at low capillary number and drying at low drying rate have been evidenced. In particular, it has been shown that the drying front and the drainage front are the very same fractal object. This also holds in the presence of gravity forces. In that case, the front has a finite thickness resulting from the equilibrium between the capillary and the gravity forces. The front thickness as well as the maximum size of the clusters that appear during drainage or drying obey scaling laws that are derived from the gradient percolation approach. However, the drying invasion front should be distinguished from the evaporation front which roughly forms the boundary between the invasion front-disconnected cluster region and the dry region. Accordingly the diffusive transport in the gas phase is very small within the cluster region.

In the absence of gravity forces, the simulations clearly show that drying of an initially saturated capillary porous medium cannot be described according to the classic continuum approach to porous media since the size of the liquid clusters may be of the order of the size of the system. In other words, no length scale separation between the size of the humidity heterogeneities and the size of the system can be expected except towards the final stages of the process when the cluster size becomes small relative to the size of the system. In the presence of gravity forces, as the process is characterized by a moving two-phase zone of finite thickness, a macroscopic approach is possible, at least for the simple geometry considered in this paper and in the limit of sufficiently large Bond numbers, i.e. when the front thickness is small relative to the system size. Under these circumstances, the problem takes a form close to the classic Stefan diffusion tube problem.

Naturally, viscous effects and temperature gradients that are not taken into account in the present approach may modify the overall picture of the process described in this paper. However, at least for drying at low drying rate, these effects are believed to modify only some details but not the main features of our results. Also, the simulations presented in this paper are restricted to two-dimensional networks. More realistic predictions could be obtained by means of a three-dimensional simulator. However, some results are such that the analogy between the drying front and the drainage invasion front undoubtedly holds in three dimensions. This allows one to take advantage of the numerous results concerning the structure of the invasion front in three dimensions [see, for instance, Gouyet *et al.* (1988)].

Acknowledgements—Financial support from Institut Français du Pétrole is gratefully acknowledged.

REFERENCES

Bird, R. B., Stewart, W. E. & Lightfoot, E. N. 1960 *Transport Phenomena.* Wiley, New York.

Birovljev, A., Furuberg, L., Feder, J., Jossang, T., Maloy, K. J. & Aharony, A. 1991 Gravity invasion percolation in two dimensions: experiment and simulation. *Phys. Rev. Lett.* **67,** 584–587.

Chandler, R., Koplik, J., Lerman, K. & Willensen, J. F. 1982 Capillary displacement and percolation in porous media. *J. Fluid Mech.* **119,** 249–267.

Clement, E., Baudet, C. & Hulin, J. P. 1985 Multiple scale structure of non wetting fluid invasion fronts in 3D model porous media. *J. Phys. Lett.* **46,** L-1163–L-1171.

Clement, E., Baudet, C., Guyon, E. & Hulin J. P. 1987 Invasion front structure in a 3D model porous medium under a hydrostatic pressure gradient. *J. Phys. D: Appl. Phys.* **20,** 608–615.

Furuberg, L., Feder, J., Aharony, A. & Jossang, T. 1988 Dynamics of invasion percolation. *Phys. Rev. Lett.* **61,** 2117–2120.

Gouyet, J. F., Rosso, M. & Sapoval, B. 1988 Fractal structure of diffusion and invasion fronts in three-dimensional lattices through the gradient percolation approach. *Phys. Rev. B* **37,** 1832–1838.

Hulin, J. P., Clement, E., Baudet, C., Gouyet, J. F. & Rosso, M. 1988 Quantitative analysis of an invading-fluid invasion front under gravity. *Phys. Rev. Lett.* **61,** 333–336.

Keey, R. B. 1972 *Drying Principles and Practice*, pp. 210–269. Pergamon Press, Oxford.

Lenormand, R., Touboul, E. & Zarcone, C. 1988 Numerical models and experiments on immiscible displacement in porous media. *J. Fluid Mech.* **189,** 165–187.

Maneval, J., McCarthy, M. J. & Whitaker, S. 1991 Studies of the drying process by NMR imaging. In *Drying 91*, pp. 170-180. Elsevier, Amsterdam.

Masmoudi, W., Prat, M. & Bories, S. 1992 Drying: percolation theory or continuum approach. Some experimental evidences. In *Heat and Mass Transfer in Porous Media* (Edited by Quintard, M. & Todorovic, M.), pp. 817–828. Elsevier, Amsterdam.

Morel, D. D., Bourbiaux, B., Latil, M. & Thiebot, B. 1990 Diffusion effects in gas flooded light oil fractured reservoirs. SPE paper 20516.

Prat, M. 1993 Percolation model of drying under isothermal conditions in porous media. *Int. J. Multiphase Flow* **19,** 691–704.

Sapoval, B., Rosso M. & Gouyet J. F. 1985 The fractal nature of a diffusion front and the relation to percolation. *J. Phys. (Paris) Lett.* **46,** L149–L156.

Shaw, T. M. 1987 Drying as an immiscible displacement process with fluid counterflow. *Phys. Rev. Lett.* **59,** 1671–1674.

Stauffer D. & Aharony, A. 1992 *Introduction to Percolation Theory*. Taylor & Francis, London.

Whitaker, S. 1977 Simultaneous heat, mass and momentum transfer in porous media. A theory of drying. In *Advances in Heat Transfer*, Vol. 13. Academic Press, New York.

Wilkinson, D. 1984 Percolation model of immiscible displacement in the presence of buoyancy forces. *Phys. Rev. A* **30,** 520–531.

Wilkinson, D. & Willemsen, J. F. 1983 Invasion percolation: a new form of percolation theory. *J. Phys. A: Math. Gen.* **16,** 3365–3376.